Computational and Structural Biotechnology Journal 23 (2024) 3132–3142

Contents lists available at ScienceDirect

Computational and Structural Biotechnology Journal

journal homepage: www.elsevier.com/locate/csbj

Research article

Crystal structure of Kunitz-type trypsin inhibitor: Entomotoxic effect of native and encapsulated protein targeting gut trypsin of *Tribolium castaneum* Herbst

Sohaib Mehmood [a], Soren Skou Thirup [b], Sarah Ahmed [c], Nabila Bashir [d], Ahsan Saeed [a], Maria Rafiq [a], Qamar Saeed [c], Muhammad Najam-ul-Haq [d], Binish Khaliq [e], Muhammad Ibrahim [f], Wadi Brak Alonazi [g], Ahmed Akrem [a,*]

[a] *Institute of Botany, Bahauddin Zakariya University, Multan 60800, Pakistan*
[b] *Department of Molecular Biology and Genetics, Centre for Structural Biology, Aarhus University, Aarhus 8000, Denmark*
[c] *Department of Entomology, Bahauddin Zakariya University, Multan 60800 Pakistan*
[d] *Institute of Chemical Sciences, Bahauddin Zakariya University, Multan 60800 Pakistan*
[e] *Botany Department, University of Okara, Okara 56300, Pakistan*
[f] *Department of Biosciences, COMSATS University Islamabad (Sahiwal Campus), Sahiwal 57000, Pakistan*
[g] *Health Administration Department, College of Business Administration, King Saud University, P. O. Box 800, Riyadh 11421, Saudi Arabia*

ARTICLE INFO

Keywords:
Albizia procera
Kunitz–type trypsin inhibitor
Crystal structure
Graphene nanoparticles
Zinc oxide nanoparticles

ABSTRACT

Trypsin inhibitors are known to act against insect pests by inhibiting proteases of the digestive tract. In this study, we report structural and functional characterization of ~ 19 kDa *Albizia procera* Kunitz-type trypsin inhibitor (ApKTI) protein with potential bio-insecticidal applications. Crystal structure of ApKTI protein has been refined to 1.42 Å and molecular structure (8HNR) showed highly beta sheeted conformation including 12 beta sheets, 15 loops and two small alpha helices. Docking between predicted model of *Tribolium castaneum* trypsin (TcPT) and 8HNR produced a stable complex (−11.3 kcal/mol) which reflects the inhibitory potential of ApKTI against insect gut trypsin. Significant mortality was observed in all life stages of *T. castaneum* including egg, larvae, pupae and adults with a 3.0 mg native ApKTI treatment in comparison to negative control. Although standard trypsin inhibitor (*Glycine max* trypsin inhibitors; GmKTI; 3.0 mg) produced maximum reduction against all above life stages; however, a non-significant mortality difference was observed in comparison to 3.0 mg native ApKTI. The study further explores the synthesis and characterization of Graphene (GNPs) and Zinc oxide (ZnONPs) nanoparticles, followed by the optimization of ApKTI and GmKTI loading on both nanoparticles to evaluate their enhanced insecticidal effectiveness. Encapsulated proteins showed significant mortality against *T. castaneum* across all concentrations, with GNPs proving more effective than ZnONPs. Additionally, encapsulated GmKTI produced significant mortality of eggs compared to loaded ApKTI treatments while other life stages were non-significantly affected by two proteins. This research highlights the importance of encapsulated ApKTI protein for eco-friendly pest management strategies.

1. Introduction

Grain crops are the dominant source of nutrition for the majority of the world's population, particularly in developing nations. Significant grain losses are incurred due to insect pests during storage [1]. Economic losses ranges between 2 to 5 % of the commercial value from a single infestation [2]. Additionally, indiscriminate use of synthetic pesticides produces even more deleterious effects such as environmental pollution, killing of non-target organisms, pest resurgence, genetic variation in plants and negative impacts on biodiversity [3]. The adverse consequences related to the inappropriate and overuse of chemical pesticides have necessitated the need for alternative means of pest management [4,5]. Thus, there is a greater focus on the development and research of botanical pesticides.

Botanical pesticides are efficacious in managing different crop pests, inexpensive, easily biodegraded, have varied modes of action, their

* Corresponding author.
E-mail address: ahmedakrem@bzu.edu.pk (A. Akrem).

https://doi.org/10.1016/j.csbj.2024.07.023
Received 18 April 2024; Received in revised form 31 July 2024; Accepted 31 July 2024
Available online 3 August 2024

sources are easily available and have low toxicity to non-target organisms. Their varied modes of action are attributed to the phytochemical composition in different plants. Therefore, they can be incorporated into integrated pest management systems and contribute to sustainable agricultural production [6]. Among them, serine PIs are the most studied and are widely present in legumes, where two types have been identified as Kunitz and Bowman-Birk trypsin inhibitors [7,8]. Kunitz inhibitors are widely distributed in plants and exhibited defense mechanisms by protecting them against insects by interfering with the digestion of proteins (inhibit trypsin activity) in insect guts, adversely affecting nutrition, growth, and metabolism [9].

In recent years, nanotechnology has also provided strong technical support and innovative ideas for agricultural development [10,11]. Nanotechnology can be applied to optimize the physical and chemical properties of pesticides, enhance pesticide delivery and promote sustained pesticide release [12,13]. Recently, a series of nanomaterials have been developed as carriers of synthetic/botanical pesticides and fertilizers [14,15]. The active ingredients (AIs) of most traditional pesticides are hydrophobic and can be encapsulated in or attached to the peripheral groups of nanoparticles, increasing the dispersion and affinity of pesticides and expanding the contact area of targets [16,17]. Graphene nanoparticles (GNPs), carbon-based nanoscale particles, have attracted tremendous attentions in drug delivery system due to its unique physical and chemical properties [18]. Graphene is a two-dimensional single layer constituted of sp2-hybridized carbon, which could supply an excellent drug-load ability with its high specific surface area [19]. On the other hand, zinc oxide nanoparticles (ZnO NPs) have been widely used in nanotechnology due to their antibacterial, antifungal, UV filtering properties, high catalytic and photochemical activity [20].

Bioinformatics, or in silico biology, is a rapidly growing field that encompasses the theory and application of computational approaches to model, predict, and explain biological function at the molecular level [21]. In-silico approaches can reduce the number of potential compounds from hundreds of thousands to the tens of thousands which could be studied for drug discovery and this results in savings of time, money and human resources [22]. Thus, present study aimed at identification, purification and three dimensional (3D) molecular structure determination of *Albizia procera* Kunitz-type trypsin inhibitor (ApKTI). Furthermore, purified ApKTI was encapsulated in graphene and ZnO nanoparticles to prevent it from leaching out before reaching the targeted site of the insects. And, 3D structure (8HNR) was docked to bovine trypsin to highlight real time interactions between plant inhibitor and insect gut trypsin.

2. Materials and methods

2.1. Extraction and purification of ApKTI

Fully mature seeds of *Albizia procera* were collected from botanical garden of Bahauddin Zakariya University, Multan, Pakistan. Common scissor was used to separate endosperm from seed coat before protein extraction. Endosperm was finely grinded by using pestle and mortar. Powder (5.0 g) was stirred for one hour in 50 ml of extraction buffer (100 mMTris-HCl; pH-7.6; 150 mM NaCl) at room temperature. Slurry was centrifuged (3345g; 30 min; 4 ºC), seed debris was discarded and protein solution (40 ml) was subjected to 60 % ammonium sulfate saturation constant. Supernatant was collected and dialyzed overnight against same buffer by using dialysis membrane (MWCO, 3.5 kDa; Spectra/Por 3). Dialyzed sample (60 ml) was filtered by using syringe filter (Q Max, Frisenette) of 0.45 μm pore size and buffer solutions (Buffer A: extraction buffer, Buffer B: extraction buffer plus 1.0 M NaCl) were filtered by passing through cellulose acetate membrane filter (0.2 μm, Sartorius Stedim Biotech, Germany). Filtered sample was loaded on Hi Trap Q FF anion exchange column (7.0 mm × 25 mm) (Cytiva life sciences) by using peristaltic pump (Miniplus 3, Gilson) which was subjected to ÄKTA prime plus FPLC (GE Healthcare). Linear gradient (0−100) of buffer B was used for protein elution at 1 ml/min flow rate. Fractions containing maximum target proteins were pooled together after SDS-PAGE analysis (Super PAGE, Bis-Tris, 10 × 8) [23]. Five millilitres of concentrated sample was loaded onto a gel filtration column Hi-Load Superdex 16/600 GL (GE Healthcare). The column was equilibrated and eluted with extraction buffer at the flow rate of 0.5 ml/min. Protein fractions with pure ApKTI were pooled together and stored at 4 ºC for further analysis. Protein quantification was determined by using Nanodrop (NanoDrop™ 2000/2000c Spectrophotometers) [24].

2.2. LC-MS/MS mass spectrometry

Stained ApKTI bands (5 kDa) were excised from the gel and reduced by using 10 mM dithiothreitol (DTT) at 55 °C for 30 min. These bands were subjected to overnight digestion through trypsin as per standard protocol [25]. The digested pieces were treated with 50% (v/v) acetonitrile and 5% (v/v) formic acid and dried in a vacuum concentrator. The calculations of LC-MS/MS were obtained by injecting protein samples onto a nano liquid chromatography system (Dionex ultimate 3000) along with an electrospray ionization ion source of an orbitrap mass spectrometer (Orbitrap FusionTM Germany). Protein sample was poured on a trapping column (Acclaim PepMap C18 75 μm × 2 cm; buffer A: 0.1% formic acid in H_2O; buffer B: 0.1% formic acid in acetonitrile) with 2.0% buffer B, peptides were eluted (300 nl min^{-1}) against the separation column. LC-MS/MS analysis was done in data dependent acquisition (DDA) MS raw data were analysed by Proteome Discoverer 2.0 (Thermo Scientific, Germany). For protein identification, MS/MS spectra were searched with Sequest HT against Arabidopsis and UniprotKB databases along with following parameters; precursor mass tolerance and fragment mass tolerance were set to 10 ppm and 0.5 respectively. Two missed cleaves were allowed while variable modification of methionine oxidation and fixed modification of carboxymethyl at cysteins were also used.

2.3. Crystallization and X-ray data collection

After identification, pooled fractions of ApKTI were concentrated up to 5 mg/ml through protein concentrator (Pierce™ Protein Concentrator PES, 10,000 MWCO, 2–6 ml) assembly and 192 crystallization conditions were set up manually by using commercially available kits comprising of different PEG (Rx1; HR2–082 & Rx2; HR2–084) and Salt (Rx1; HR2–107 & Rx2; HR2–109) recipes (Hampton Research). Sitting drop vapor diffusion method was used by mixing 1 μl of protein sample with 1 μl of reservoir solution (200 μl) and MRC Maxi 48-well crystallization plates (Hampton Research) were sealed and stored at 20 °C. Plates were observed very carefully under stereomicroscope (Leica, MZ 12.5) on daily basis. After obtaining initial crystallization conditions (0.1 M MES monohydrate (pH: 6.0), PEG 400 (22%), the crystallization conditions were optimized by varying the percentage of principle reservoir ingredient. Promising crystallization conditions were refined by the same sitting drop method in 24 well Cryschem plates (Hampton Research) and crystallization drops were made by 1 μl of protein sample plus 1 μl of reservoir solution (500 μl). The plates were sealed and stored at 20 °C. After effective optimization of crystallization conditions, the final condition for Kunitz-type trypsin inhibitor was 0.1 M MES monohydrate (pH: 6.0), PEG 400 (25%). Single crystal was fished using a 0.2 mm litho loop and flash cooled in liquid nitrogen and stored in Spinepucks for safe transfer to the beamline P13 operated by EMBL Hamburg at the PETRA III storage ring (DESY, Hamburg, Germany). X-ray standard data were collected at 100 K and crystal to detector distance was set at 140.84 mm. 0.1° rotation images covering a full 360° rotation of the crystals were recorded on a DECTRIS EIGER 16 M detector.

2.4. Data processing and molecular structure refinement

The X-ray diffraction data were processed, indexed, merged, and scaled with XDS and XSCALE [26]. Phase information was obtained by using coordinates of already reported *Enterolobium contortisiliquum* trypsin inhibitor (PDB: 4J2K) using Molecular Replacement in *Phenix* [27]. The initial molecular replacement model was model build in Coot [28] replacing residues of the *E. contortisiliquum* sequence were this was suggested by the difference electron density. The model was refined to 1.42 Å resolution using phenix refine alternating with model building in Coot and further replacing residues when suggested by the difference electron density. Each refinement step was composed of nine macro-cycles, and included, refinement of individual atomic coordinates using gradient driven minimization and individual isotropic B-factors. Furthermore, water molecules were placed automatically by *Phenix*. Translation, liberation and screw motion (TLS) were not included in the refinement strategy as it did not improve the R-values. The structure quality was assessed with MOLPROBITY and POLYGON from the *phenix*. Data collection and refinement statistics is summarized in Table 2.

2.5. Modelling and molecular docking studies

The amino acid sequence of *T. castaneum* trypsin (XP_008200977.1) was retrieved from NCBI (https://www.ncbi.nlm.nih.gov/) and used as input for automated modelling server SWISS- MODEL (https://swissmodel.expasy.org/). The model (*T. castaneum* Predicted Trypsin; TcPT) was built using PDB entry 1OPH (bovine trypsin) as a template, having 38 % sequence identity and a coverage of 83 % amino acid residues. Insect model (TcPT) was subsequently used for docking studies with ApKTI (8HNR) using ClusPro 2.0 webserver (https://cluspro.org), a widely used tool for protein-protein docking [29]. Enzyme (Trypsin) was selected as a receptor while inhibitor (ApKTI) as a ligand providing A and B as the Chain IDs. As soon as the job showed up on the Queue page, status was checked. Status page showed the job name, job ID number, job status, PDB ID and submission time stamp. ClusPro 2.0 follows three main computational steps: first step is running docking program (PIPER) that performs systematic search of complex conformations using fast Fourier transform (FFT), second step is clustering of the generated structures based on pairwise root mean square deviation (RMSD) as the distance measure and third step is the refinement of the selected structures. When the job was completed, the Result page displayed pictures of 10 models (centers of the ten most populated clusters) by default. Docked files were downloaded and uploaded on to PDBsum to generate full set of structural analysis and list of interactions (http://www.ebi.ac.uk/thornton-srv/databases/pdbsum/Generate.html). Then, docked complex was uploaded on PRODIGY (https://wenmr.science.uu.nl/prodigy/) web server to investigate the protein-protein interface interactions. Docked pdb files were also opened in PyMol software (The PyMol Molecular Graphics System, Version 2.0 Schrödinger, LLC)) to highlight various types of interactions and for cartoon presentations.

2.6. Inhibitory activity against trypsin

Trypsin inhibitory assay was performed to check inhibition activity of purified ApKTI using Nα-benzoyl-DL-arginine-p-nitroanilide (BApNA; Sigma-Aldrich) as a substrate. In this assay, 2.5 μg bovine trypsin (Sigma-Aldrich) was calculated from stock solution (5 mg/10 ml) and mixed with Tris-HCl (100 mM, pH: 7.6) and incubated at 37 °C for 15 min along with different concentrations of ApKTI which were obtained after each purification step (Table 1). Reaction began with the addition of 500 μl of 1.25 mM Nα-benzoyl-DL-arginine-p-nitroanilide (pre-warmed, 37 °C) solution. Then, the reaction mixture (3 ml) was vortexed and incubated for 10 min. At the end, reaction was terminated by addition of 30 % acetic acid (100 μl) and reaction mixture was centrifuged at 1000g for 5 min. Optical density of supernatant for substrate hydrolysis was measured at 410 nm and readings rectified for blank. Specific activity and total inhibitory activity was also calculated [30].

Table 1
Purification of ApKTI from five grams of *A. procera* seeds.

Steps	Total water soluble protein (mg)	Total activity (TIU) × 10^5	Specific activity (TIU) × 10^5	Yield (%)	Purification (fold)
Crude extract	352.5	13.56	0.038	100	1
Ammonium Sulfate	223.37	9.14	0.040	67	1.05
Ion exchange	94.06	4.07	0.043	30	1.13
Gel filtration	16.5	0.95	0.057	7.0	1.5

2.7. Insect collection

Insect culture of *Tribolium castaneum* were obtained from grain market, Multan, Pakistan (30.1751° N, 71.4693° E) and reared at Eco-toxicology laboratory, Entomology Department, Bahauddin Zakariya University, Multan, Pakistan (30° 11′44 N; 71° 28′ 31 E). *T. castaneum* cultures were maintained on *Triticum aestivum* (wheat grains) (35 ± 5 °C; 65 ± 5 % RH). *T. castaneum* adults were separated at pupal stage on the basis of sex as per standard protocol [31].

2.8. Feeding toxicity

For entomotoxic activity of trypsin inhibitors against *T. castaneum*, three concentrations (1.0, 2.0 and 3.0 mg) of ApKTI, Standard protein as positive controls (*Glycin max* trypsin inhibitors; GmKTI; Cat. Nos. T2327; Sigma Aldrich) and corresponding extraction buffer as negative control were mixed with 200 g of wheat flour. Each treatment (40 g/replicate) was replicated five times and each replicated treatment was performed in separate jar. Five newly emerged adult pairs of *T. castaneum* were placed in their respective experimental unit at 35 ± 5 °C and 65 ± 5 % RH. After ten days, adults were removed and data were observed weekly to examine the change in life cycle parameters (number of eggs, larvae, pupae and adult emergence) of *T. castaneum*.

2.9. Synthesis of Graphene and Zinc oxide nanoparticles

Graphene nanoparticles (GNPs) were produced from pure graphite powder using modified Hummer's method [32] in which graphite powder (2.0 g) was mixed with sulfuric acid (18.4 M; 120 ml) and stirred for 30 min in an ice bath. Potassium permanganate (11.6 g) was added slowly and stirred the solution for two hours at 30 °C. Then, deionized water (80 ml) was added and raised the temperature to 90 °C for 30 min. After that, temperature of the solution brought to 60 °C and again deionized water (160 ml) was added. Then, H_2O_2 (30 %) was dropped slowly to get an orange yellow solution. Next, 5 % HCl (400 ml) solution was added to maintain pH at 5.0 by washing through the vacuum pump and graphene oxide (blackish grey) was obtained. Graphene oxide (1.0 g) was agitated with H_2SO_4 (20 ml) in an ice bath for two hours. Then, 50 % $KMnO_4$ (10 ml) was added and solution was stirred for two hours and after that, temperature was raised to 50 °C for one hour. Additionally, distilled water (80 ml) was added and temperature was raised to 90 °C for 30 min. After $KMnO_4$ homogenization, 20 ml hydrogen peroxide (H_2O_2) added to the ice bath followed by the addition of distilled water until the appearance of a yellow brown colour solution. At the end, solution was ultrsonicated and pH was increased to 8 and then lowered to 4, getting a dark greenish yellow mixture.

On the other hand, zinc oxide nanoparticles (ZnONPs) were prepared by precipitation method using zinc sulfate ($ZnSO_4$) and sodium

hydroxide (NaOH) as raw materials. To the aqueous solution of zinc sulfate, sodium hydroxide was mixed dropwise in molar strength of 1:2 under robust stirring which was continued for 12 h. The resultant mixture was filtered and washed properly with deionized water. Then, the mixture was dried in an oven (100 °C) and ground to fine powder using pestle mortar. At the end, the powder was calcined at different temperatures (300 °C, 500 °C, 700 °C, 900 °C) for 2 h [33].

These nanoparticles were characterized by Fourier Transform Infrared Spectroscopy (FTIR), X-ray Diffraction analysis (XRD) and Scanning Electron Microscopy (SEM).

2.10. Optimization of nanoparticles encapsulation

Encapsulation of graphene and zinc oxide nanoparticles (GNPs and ZnONPs) was optimised by using different parameters like concentration, temperature and time. To optimize protein concentration, different solutions (~ 10, 20, 30, 40, 50 and 100 mg/l) of commercial trypsin inhibitor from soybean (Kunitz; GmKTI) were prepared from stock solution (~ 1000 mg/l). These concentrations were used against 0.05 g nanoparticles at 25 °C and for one hour stirring time. Different weights (0.025, 0.05, 0.1 and 0.2 g) of both nanoparticles were optimized against a single concentration (100 ppm) of standard protein at 25 °C and for one hour stirring time. Similarly, various temperatures (4.0, 25 and 50 °C) were used against 100 ppm protein solution with 0.05 g nanoparticles and one hour stirring time. Additionally, several stirring timings (30 min, 1.0 h and 2.0 h) were optimized against 100 ppm protein solution with 0.05 g nanoparticles at 25 °C. Encapsulation efficiency (EE) was calculated using following formula:

$$\text{Encapsulation efficiency\%} = \frac{\text{Total protein} - \text{free protein after encapsulation}}{\text{Total protein}} \times 100$$

2.11. Insecticidal activity of encapsulated proteins and data analysis

ApKTI and standard protein (GmKTI) were encapsulated with both nanoparticles and subjected to insecticidal assay at optimized conditions (Table 3) against *T. castaneum* at same three doses (1.0, 2.0 and 3.0 mg) and method (feeding toxicity) as discussed above. To observe changes in the life parameters of insect, data was observed on weekly basis. Data was further analyzed by ANOVA using Statistics 8.1 [34].

3. Results

3.1. Purification and electrophoretic analysis

Purified protein (ApKTI) was obtained from gel filtration chromatography (Hi-Load Superdex 16/600 GL) after ammonium sulphate precipitation (60 %) and followed by ion exchange chromatography (Hi Trap Q FF anion exchange column) (Fig. 1A). In a thorough purification experiment, approximately 16.5 mg of ApKTI was obtained from five grams of endosperm. Highly purified ApKTI (after gel filtration) exhibited a specific activity of 0.057×10^5 TIU/mg, a purification fold of 1.5 and a yield of 7.0 % (Table 1). SDS-PAGE analysis of ApKTI showed a single band with an apparent molecular weight of 19 kDa under non reduced condition (without β-mercaptoethanol). However, under reduced condition (with β-mercaptoethanol), ApKTI demonstrated two corresponding bands of 14 and 5 kDa indicating the presence of inter chain disulfide linkage (Fig. 1B & 1 C). LC/MS-MS generated a single fragment comprising of 12 residues and BLAST result confirmed the identification of protein as ApKTI (Fig. S1).

3.2. Quality of crystal structure of ApKTI

X-ray diffraction data collection at 100 K from a single needle shaped crystal (Fig. S2) of ApKTI resulted in a dataset extending to 1.42 Å resolution. The space group was found to be C2 with unit cell dimensions a = 120.63 Å, b = 34.97 Å, c = 42.70 Å, and β = 104.74°. The data, refinement statistics, and model quality parameters are summarised in Table 2. The final model of ApKTI contains one inhibitor molecule and 170 water molecules in the asymmetric unit. The model is in good agreement with ideal geometry with low RMS deviation of bond angles (1.08°), bond length (0.011 Å), and no residues within the disallowed regions of the Ramachandran plot. During model building, 21 and 31 residue side chains of the molecular replacement model was replaced to obtain a better agreement with the observed electron density (Fig. S3). The final ApKTI model (Fig. 2) was refined to an R-factor of 16.2 % and R_{free} of 18.5 %. All coordinate information have been deposited at the

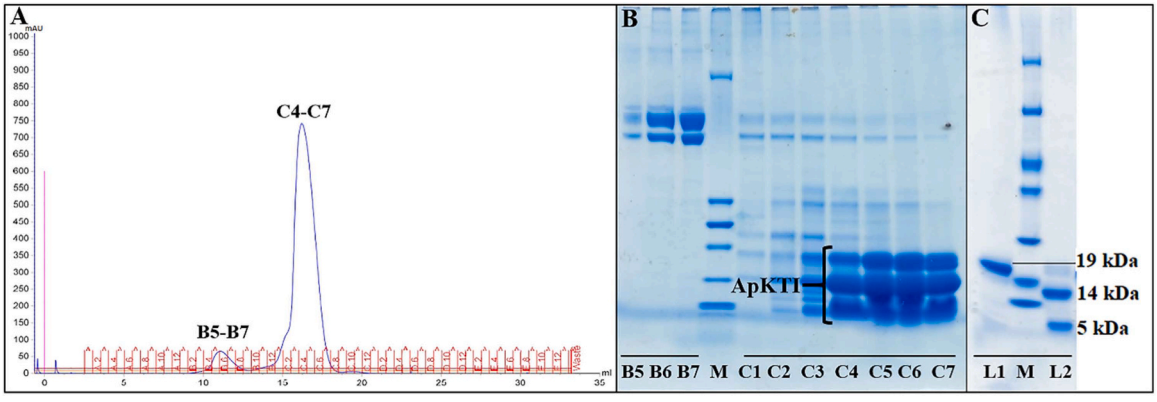

Fig. 1. : Gel filtration chromatogram and corresponding SDS-PAGE analysis of ApKTI. A is Superdex 200 increase gel filtration chromatogram of ApKTI where C4-C7 are the fractions comprising of pure ApKTI. **B** is the corresponding SDS-PAGE along with standard protein ladder 'M' (Catalog no. 26632) and exhibiting the banding pattern of vicilin (B5-B7) as well as highly pure ApKTI fractions (C4-C7). **C** is showing optimized and diluted concentration of ApKTI under non-reduced (L1; 19 kDa) and reduced (L2; 14 & 5 kDa) conditions along with protein marker (Catalog no. 26610).

Table 2
Data collection and refinement statistics.

Sr. no.	Metrics	Values
1	Wavelength (Å)	1.42
2	Resolution range (Å)	41.3 - 1.422 (1.472 - 1.422)*
3	Space group	C 1 2 1
4	Unit cell *a*, *b*, *c* (Å)	120.63, 34.97, 42.70
	α, β, γ (°)	90, 104.74, 90
5	Completeness (%)	98.31 (96.07)
6	Mean I/sigma (I)	14.17 (1.27)
7	CC1/2	0.999 (0.765)
8	R-work	0.162 (0.3212)
9	R-free	0.185 (0.3558)
10	Clash score	4
11	Ramachandran favoured (%)	95.68
12	Ramachandran allowed (%)	4.32
13	Average B-factor	30.83
14	Protein residues	166
15	Ligand	0
16	RMS (bonds) Å	0.011
17	RMS (angles) Å	1.08

* Statistics for the highest-resolution shell are shown in parentheses.

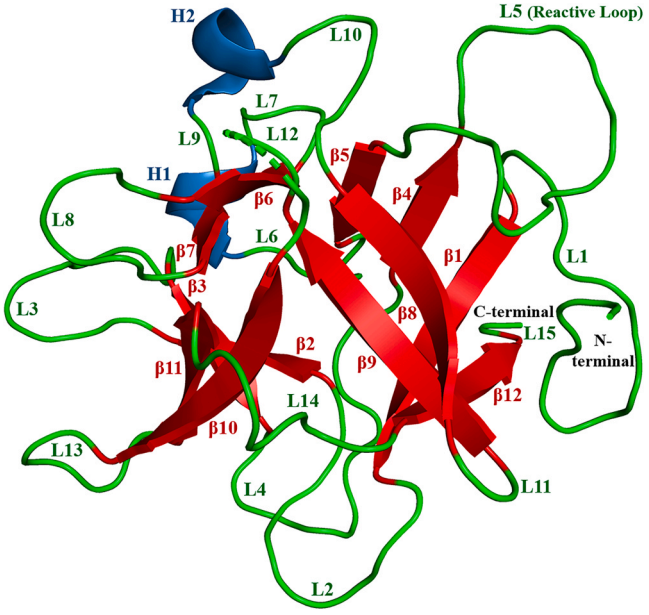

Fig. 2. : Cartoon representation of three dimensional crystallographic structure of ApKTI. Beta sheets are labelled as *β*1-*β*12 (red), loops as L1-L15 (green) and alpha helices as H1-H2 (blue). Loop L10 is only marked for consistency with the other related structures, since the main chain is broken in this region. Loop 12 the point of detachment (NS) that splits the 19 kDa protein into two polypeptides of 14 & 5 kDa.

RCSB Protein Data Bank under PDB ID: 8HNR.

3.3. Description of ApKTI (8HNR) 3D structure

The fold of ApKTI is a β-trefoil which is typical for STI-related Kunitz-type trypsin inhibitors, consisting of twelve β-strands (β1- β12) along with the loops (L1 - L15) connecting these strands and two helices (H1 and H2). The reactive loop (L5) responsible for inhibitory activity against trypsin is located between β-strand 4 and β-strand 5 (Fig. 2). ApKTI molecule contains two disulfide linkages, one intra-chain and other inter-chain.The intra-chain disulfide bond (Cys 40 and Cys 86) connects loops L3 and L6 and the inter-chain disulfide linkage (Cys 133 and Cys 142) is responsible for covalently connecting the two polypeptide chains, providing additional stability to the structure. Experimentally determined structures of Kunitz-type trypsin inhibitors that share the β-trefoil fold with ApKTI; are EcTI (4J2K) from *Enterolobium contortisiliquum*, TKI (4AN6) from *Tamarindus indica* and STI (1BA7) from *Glycine max* (Fig. S4). Superposition of ApKTI with EcTI, TKI and STI, showed high structural similarity for the core of the beta trefoil structure with respective RMSD values of 0.268 Å for 132 pairs of superimposed Cα atoms of EcTI, 0.664 Å for 108 atom pairs of TKI and 0.590 Å for the 110 atom pairs of STI. However, significant differences are found among loop regions. Additionally, ApKTI (8HNR) showed sequence identities of 87 %, 86 %, 43 % and 34 % with EcTI, AcTI (*Acacia confusa*), TKI and STI, respectively. All the important parameters including secondary structural elements, disulfide linkages, reactive loop, reactive residues, point of detachment of two polypeptide chains and LC/MS-MS generated residual sequence are highlighted in Fig. 3.

3.4. Molecular docking between 8HNR and TcPT

The ApKTI crystal structure (8HNR) was docked with the predicted structure of *Tribolium castaneum* trypsin (TcPT) to highlight the actual interactions between enzyme and inhibitor complex within the insect gut (Fig. 4A). Molecular docking showed two salt bridges are formed between Arg-64↔Asp-211, and Arg-92↔Asp-239 (Fig. S5). Moreover, docked complex exhibited seventeen hydrogen bonding (8 residues from 8HNR and 11 residues from TcPT; Fig. 4B) and 169 non bonded interactions. In reactive loop region other contributing residues include Thr-61, Pro-62, Pro-63 and Ala-66 which form hydrogen bonds with various residues of trypsin. Additionally, Arg-92 make another salt bridge with Asp-239. ApKTI residues Arg-12, Thr-16 and Gln-79 are involved in hydrogen bonding interactions with trypsin residues. PRODIGY predicts enzyme-inhibitor complex to be highly stable based on binding energies −11.3 kcal/mol.

3.5. Feeding toxicity

T. castaneum was fed on wheat flour mixed with three doses (1.0, 2.0 and 3.0 mg) of native ApKTI, positive and negative control, the results were highly significant. There was a notable difference among mean number of eggs ($F = 42.4$, $df = 4$, $P = 0.0000$) as shown in Fig. 5. Minimum number of eggs were observed at 3.0 mg when compared with negative control while, positive control exhibited least number of eggs in comparison to all ApKTI doses. Larvae of *T. castaneum* were found statistically lower in number at positive control (40.6 ± 9.13) and highest concentration (52.2 ± 9.13) of ApKTI ($F = 358$, $df = 4$, $P = 0.0000$), whereas highest larval population were observed in negative control (451.2 ± 12.9). Interestingly, all ApKTI concentrations along with positive and negative controls showed significant differences ($F = 362$, $df = 4$, $P = 0.0000$). Least mean value was observed in positive control (35.8 ± 9.11) and at 3.0 mg (54.8 ± 9.11) while the highest in negative control (451.2 ± 12.89). Similarly, a statistically significant difference was observed in among all protein doses regarding adult emergence ($F = 350$, $df = 4$, $P = 0.0000$). The mean number of adults were similar to each other and showed difference when compared with controls.

3.6. FTIR of Graphene nanoparticles (GNPs) and ZnO nanoparticles (ZnONPs)

The FTIR spectra of the synthesized GNPs are shown in Fig. 6A. The FTIR spectrum shows the clear peaks of O–H bonding centered at 1637 cm^{-1} and a broad peak at 3402 cm^{-1}. While the spectral signatures at 1078 cm^{-1} and 1255 cm^{-1} specify the existence of C–O and C–H respectively. Signals at 2950 cm^{-1} show the absorption of C–H stretching vibrations and below 1250 cm^{-1} signify the stretching vibration of –C–O–C in G-GNPs. The GNPs sample also showed FTIR bands of skeletal vibration of aromatic rings at about 1550 cm^{-1} and stretching vibration of C–H at around 3050 cm^{-1}. Moreover, the GNPs sample exhibited a band around 3320 cm^{-1} showing the stretching vibration of

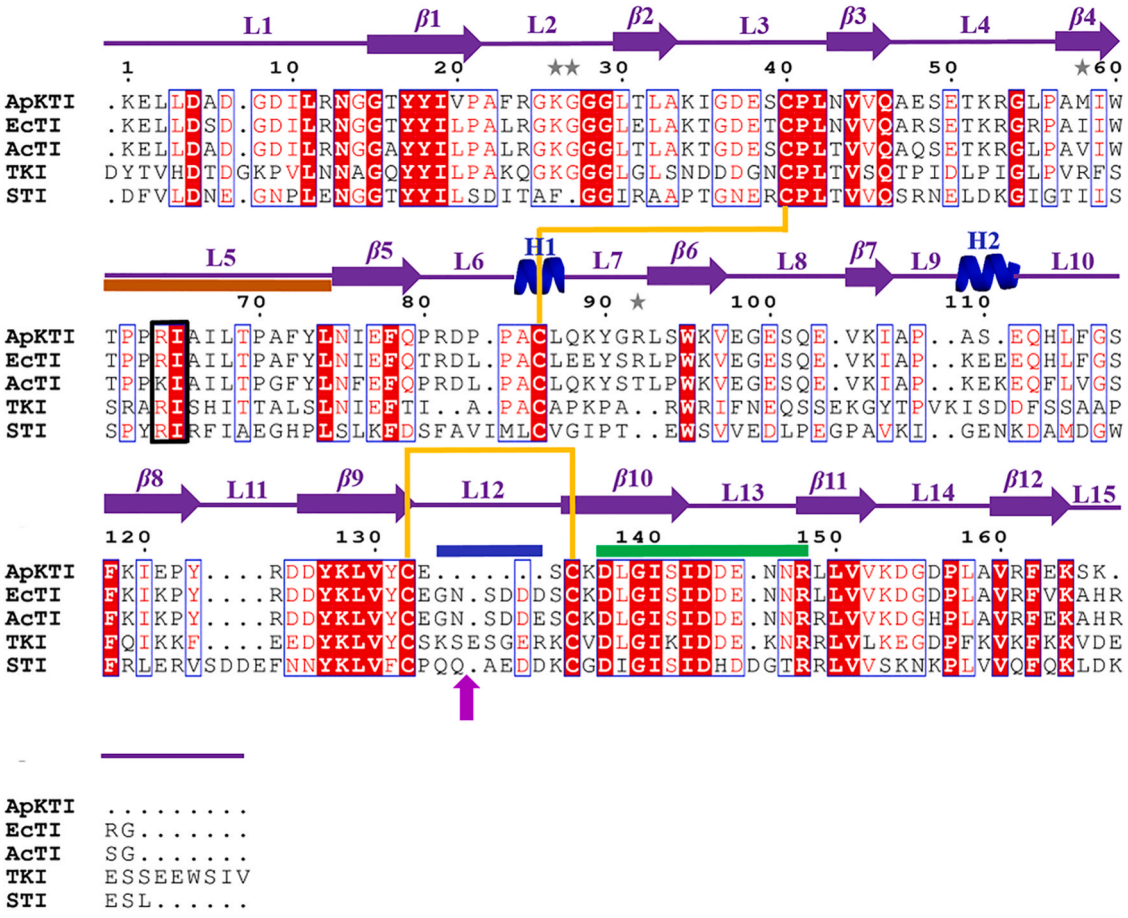

Fig. 3. : Multiple sequence alignment (MSA). MSA of structure-based sequence of ApKTI (8HNR) with *Enterolobium contortisiliquum* (EcTI: 4J2K), *Acacia confusa* (AcTI: P24924), *Tamarindus indica* (TKI: 4AN6) and *Glycine max* (STI: 1BA7) trypsin inhibitors which showed 87 %, 86 %, 43 % and 34 % sequence identity respectively. Structural elements including two α-helices, twelve β-sheets and fifteen loops are drawn at the top of alignment, yellow lines indicating highly conserved disulphide linkages, orange bar showing reactive loop and black box enclosing reactive residues. Identical amino acids are highlighted on red background while similar and dissimilar residues on white background. Purple arrow is indicating point of detachment of both chains in reducing conditions. Green bar is representing the residues generated by mass spectrometry. Blue bar is indicating six residues (GNSDDE) whose electron density did not appear and were not modelled in structure. However, they were deposited to PDB.

hydroxyl (O–H) group, whereas the signal near 2900 cm^{-1} was given to symmetric and asymmetric stretching of C–H bond [35]. The FTIR spectrum of ZnO nanoparticles is given in Fig. 6B. The FTIR spectra shows the peaks functional groups that were present in the nanoparticles. It is observed that the FTIR ZnO nanoparticles shows the bending or stretching vibrations at 685, 827, 1402 and 3376 of Zn-O, Zn-OH, -C═O (and caused by C-C known as "Fingerprint region") and -OH stretch respectively [36].

3.7. XRD of Graphene nanoparticles (GNPs) and ZnO nanoparticles (ZnONPs)

X-ray diffraction (XRD) analysis of graphene oxide nanoparticles given in Fig. 6C showed structure, phase and the crystallinity of the material. GNPs demonstrated peaks at 32.09° for Graphene oxide and 28.51° for graphite. The peaks were compared with the reported peaks given in the database of JCPDS cards (1906–29). The particle size range was calculated using the Scherer equation and was found to be 11 nm from the X-ray diffraction results. It as results, XRD confirmed the existence of synthesized graphene oxide nanoparticles [37]. Strong Bragg reflection peaks at 17.5°, 23.45°, 31.72°, 34.5°, 36.3°, 43.1°, 47.76°, and 59° are visible in Fig. 6D and reveal the existence of ZnONPs. These peaks are compared to their corresponding Miller indices, which correspond to the typical Wurtzite ZnO structure and are (100), (002), (101), (102), (110), (103), and (201), respectively. As a result, XRD examination supports the existence of synthesized ZnONPs [38].

3.8. SEM of Graphene nanoparticles (GNPs) and ZnO nanoparticles (ZnONPs)

SEM is carried out to assess the morphology of and the particle sizes of the synthesized nanoparticles. Fig. 7A indicates the SEM images of graphene oxide nanoparticles revealing the distribution and arrangement of the nanoparticles on a microscale level. The 1-micrometer scale shows the multiple nanoparticles which provide insights into how the nanoparticles are dispersed or clustered, offering information about their overall spatial organization. Fig. 7B indicates the SEM images at a higher magnification of 0.5 micrometers that shows the distribution of individual nanoparticles more clearly. This scale allows for a detailed examination of the size, shape, and structural features of each nanoparticle for understanding the homogeneity or heterogeneity of the graphene nanoparticles. It is also showing the details of the edges, defects, and other structural characteristics. Whereas, Figs. 7C and 7D show the zinc oxide nanoparticles at 1 μm and 0.5 μm scales. The images reveal that particles are in quantum size and spherical in shape and homogenous in geometry. The images at 0.5 μm scale show that all the nanoparticles are below 100 nm.

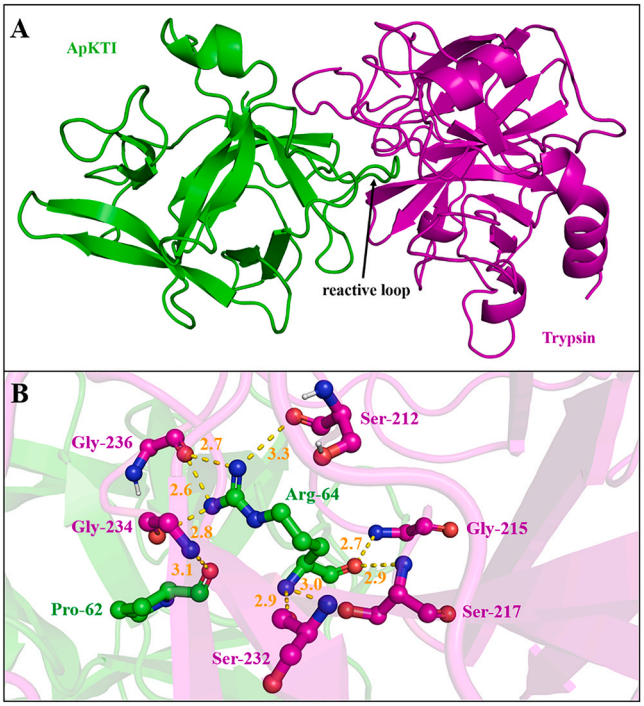

Fig. 4. : Overall structure and Hydrogen bonding of ApKTI and insect Trypsin complex. (A) Cartoon diagram is showing docked complex of 8HNR (ApKTI) and *Tribolium castaneum* predicted trypsin (TcPT). ApKTI is coloured green while trypsin is coloured magenta and the reactive loop of 8HNR is indicated. (B) Network comprising of hydrogen bonding between ApKTI and TcPT is shown.

3.9. Optimization of encapsulation conditions

ApKTI was encapsulated with GNPs and ZnONPs significantly under the conditions as mentioned in Table 3.

3.10. Feeding toxicity of nanoparticles

Optimized quantity of GNPs (0.025 g) and ZnONPs (0.5 g) were mixed with wheat flour as well as extraction buffer and fed to *T. castaneum* to evaluate their effects on life parameters. Graphene nanoparticles showed inert behaviour while zinc oxide nanoparticles exhibited a little activity as compared to control as explained in results (Fig. S6).

3.11. Feeding toxicity of encapsulated proteins

Various life cycle parameters of *T. castaneum* were observed after exposure to encapsulated ApKTI and standard GmKTI proteins. Ratios of total number of eggs, larvae, pupae and adults were calculated and remarkable reduction were observed for all parameters when compared with control. But, all treatments of both (ApKTI and standard GmKTI) proteins showed non-significant results in comparison to each other.

A significant difference was observed in total number of eggs among graphene encapsulated ApKTI ($F = 41.2$, $df = 3$, $P = 0.0000$) and ZnO encapsulated ApKTI ($F = 71.6$, $df = 3$, $P = 0.0000$) at highest concentration (3.0 mg). Larval population were found minimal in graphene encapsulated ApKTI ($F = 435$, $df = 3$, $P = 0.0000$) and ZnO encapsulated ApKTI ($F = 365$, $df = 3$, $P = 0.0000$) at highest protein dose. Least number of pupae were recorded in graphene encapsulated ApKTI ($F = 436$, $df = 3$, $P = 0.0000$) and ZnO encapsulated ApKTI ($F = 366$, $df = 3$, $P = 0.0000$) at highest protein concentration. Statistically significant reduction in adult emergence were observed at highest protein dose in graphene encapsulated ApKTI ($F = 422$, $df = 3$, $P = 0.0000$) and ZnO encapsulated ApKTI ($F = 354$, $df = 3$, $P = 0.0000$) (Fig. 8).

Similarly, a prominent difference was observed in total number of eggs among graphene encapsulated standard GmKTI ($F = 120$, $df = 3$, $P = 0.0000$) and ZnO encapsulated standard GmKTI ($F = 103$, $df = 3$, $P = 0.0000$) at highest concentration (3.0 mg). Larval population were found minimal in graphene encapsulated standard GmKTI ($F = 460$, $df = 3$, $P = 0.0000$) and ZnO encapsulated standard GmKTI ($F = 398$, $df = 3$, $P = 0.0000$) at highest protein dose. Least number of pupae were recorded in graphene encapsulated standard GmKTI ($F = 463$, $df = 3$, $P = 0.0000$) and ZnO encapsulated standard GmKTI ($F = 403$, $df = 3$, $P = 0.0000$) at highest protein concentration. Statistically significant reduction in adult emergence were observed at highest protein dose in graphene encapsulated standard GmKTI ($F = 444$, $df = 3$, $P = 0.0000$) and ZnO encapsulated standard GmKTI ($F = 385$, $df = 3$, $P = 0.0000$) (Fig. 9).

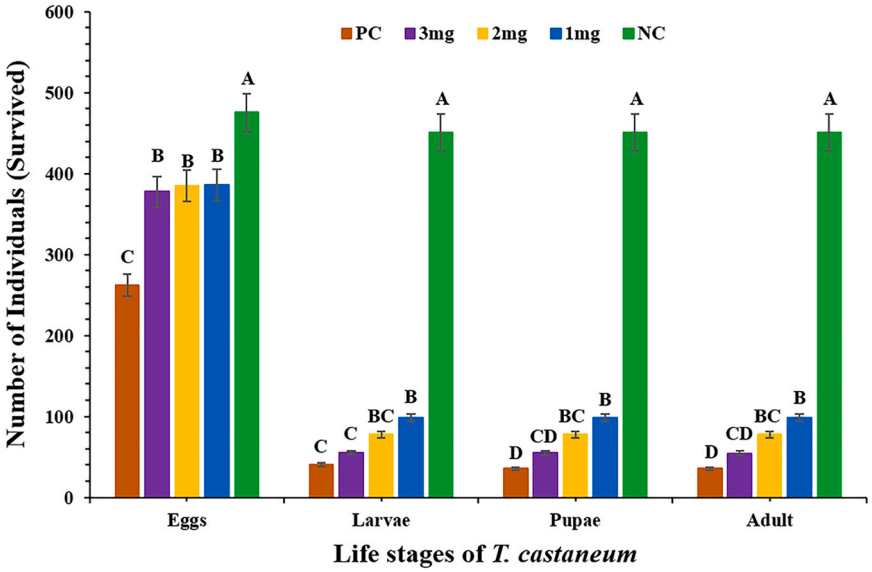

Fig. 5. : Entomotoxic activity native ApKTI against *T. castaneum*. Graph is showing the effect of three concentrations (1.0, 2.0 and 3.0 mg) of ApKTI, positive control (PC; standard trypsin inhibitor; 3.0 mg) and negative control (NC; Tris-HCl, 100 mM, pH-7.6) on different life stages of *T. castaneum*. Letters (A, B, C & D) above bars are indicating whether the treatment means are statistically significant or non-significant.

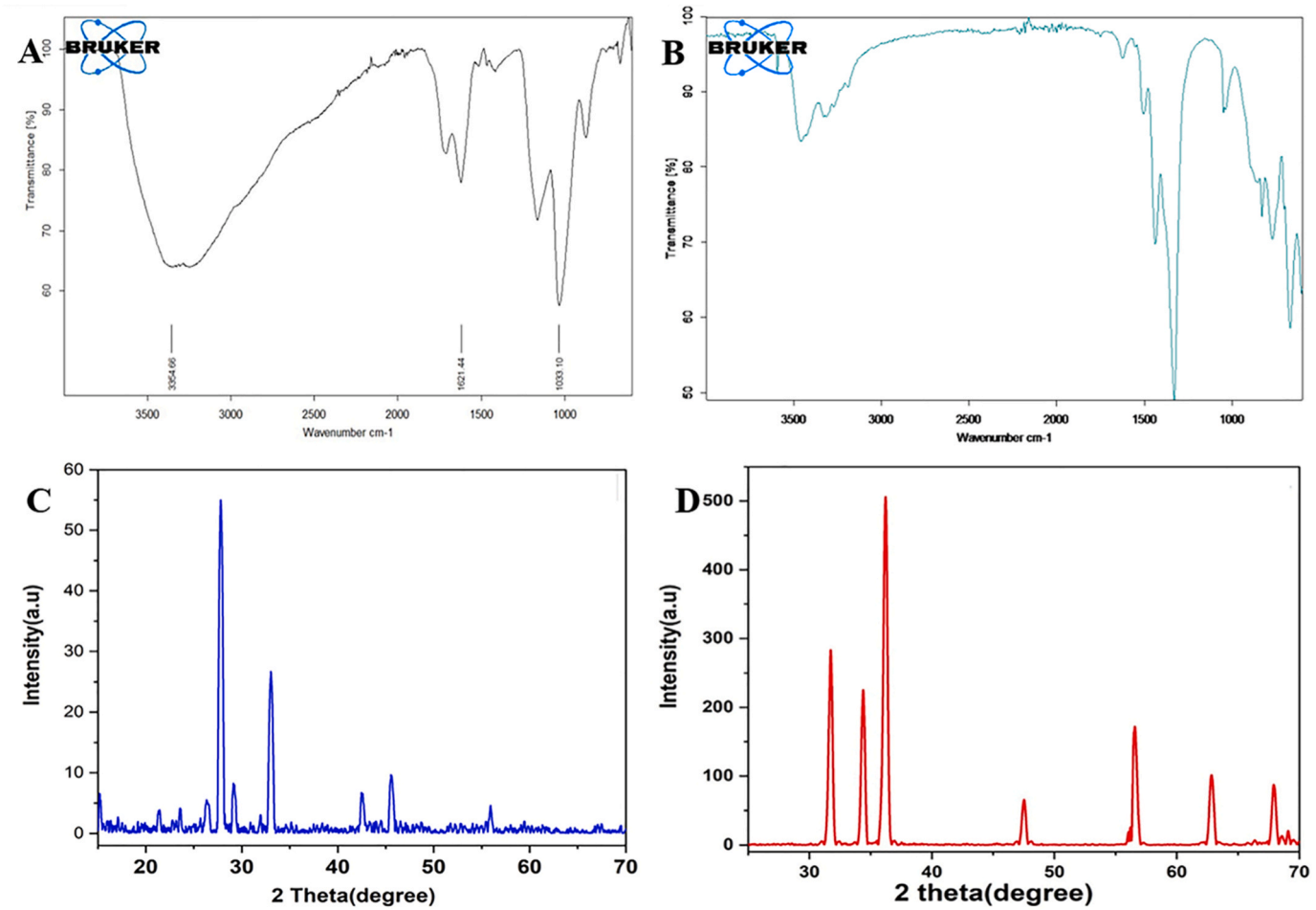

Fig. 6. : Characterization of Nanoparticles. A and B are showing the FTIR of GNPs and ZnONPs respectively. C and D is showing the XRD of GQDs and ZnOQDs respectively.

4. Discussion

Plant protease inhibitors have been studied for their potential role in defence against insects, pathogens and herbivore predation. Inhibitors targeting serine proteases such as trypsin are of particular interest due to their involvement in the nutrition, digestion and development of insects. Insecticidal activity of many protease inhibitors from various plant species have been reported. Analysis of SDS-PAGE of ApKTI revealed the presence of single band of 19 kDa under non reduced condition which cleaved into daughter bands of 14 and 5 kDa under reduced condition (Fig. 1C). This molecular weight is consistent with already reported Kunitz-type trypsin inhibitor such as EpTI, *An*TI and EcTI [39–41].

Based on the sequence identity of LC/MS-MS generated fragments and structure based sequence with already reported trypsin inhibitors, ApKTI has been classified as Kunitz-type trypsin inhibitor. Multiple sequence alignment is showing that most conserved residues are located in β strand regions which are responsible for the creation of common β-trefoil fold. Similarly, the presence of variable residues in loop regions are responsible for different biological functions to the members of KTI family. These variations may be due to deletion or insertion of residues in loops. The crystal structure of ApKTI illustrates that it possesses a β-trefoil fold similar to Kunitz-type trypsin inhibitor (STI) and the fold consists of twelve antiparallel β strands arranged into three structurally similar units related by pseudo threefold symmetry and β barrel which creates a significant hydrophobic core (Fig. 2). ApKTI have two small helices but lacks any significant helix like other KTIs. As found in most of the Kunitz-type trypsin inhibitors, ApKTI has single reactive site located between fourth and fifth β-strand which consists of fourteen residues (Thr-61-Leu-74).

Protease inhibitors that binds to trypsin and trypsin like enzymes can hinder the supply of essential amino acids and lead to starvation and eventual death. Docked complex between crystallographic ApKTI and predicted TcPT explained the inhibition mechanism of midgut trypsin enzyme. ApKTI belongs to the family of substrate like inhibitors characterized by the presence of a reactive site loop in conical conformation. Its reactive site adopts a classical non-covalent lock and key inhibitory mechanism. The presence of two consecutive proline molecules in reactive loop of ApKTI makes the sequence similar to EcTI, but different from STI and TKI; however, it does not change the conical binding mode. In comparison to two Arginines of ApKTI for two salt bridges (2 R↔2D) with TcPT, while EcTI, TKI and STI showed only one Arginine for single salt bridge formation between co-crystallized trypsin and trypsin inhibitor. Similarly, ApKTI (8 residues) showed 19 hydrogen bonding in docked complex with predicted TcPT, while EcTI (8 residues), TKI (10 residues) and STI (12 residues) formed 9, 21 and 8 bonding respectively. Side chain of ApKTI Arg-64 acts exactly like a key inserting into the active site of trypsin and makes one salt bridge, eight hydrogen bonds and 51 non bonded interactions. In comparison, key residue EcTI Arg-64 makes an ionic interaction (salt bridge) as well as six direct hydrogen bonds and three indirect hydrogen bonds with trypsin [41]. Another Kunitz-type trypsin inhibitor (TKI) from Tamarind was co-crystalized with porcine pancreatic trypsin (PPT). In TKI-PPT structure, a total of ten residues of TKI interact with twenty residues of PPT forming a dense network of hydrogen bonds to produce a stable complex. There are 21 hydrogen bonds between TKI and PPT involving four residues of the reactive site. The main residue of TKI, Arg-66, forms one salt bridge and

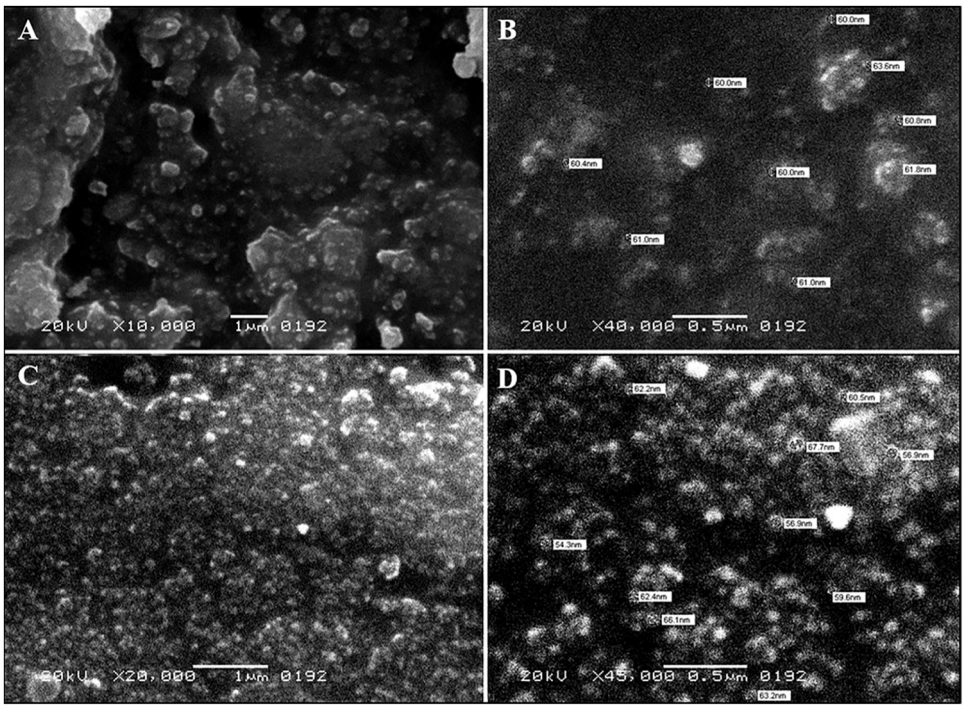

Fig. 7. : Scanning Electron Microscopy (SEM). A is the SEM of GNPs at 1 μm scale while B is the SEM of GNPs at 0.5 μm scale. Similarly, C is the SEM of ZnONPs at 1 μm scale while D is the SEM of ZnONPs at 0.5 μm scale.

Table 3
Optimization of various physical parameters for ApKTI & GmKTI encapsulation.

Parameters	Graphene	Zinc Oxide
Temperature (°C)	25	25
Stirring time (minutes)	30	60
Protein concentration (mg)	3.0	3.0
Nanoparticles concentration (g)	0.025	0.05

a large number of comprehensive hydrogen bonds with PPT [42].

Additionally, the molecular structure of a Kunitz-type trypsin inhibitor from soybean (STI) was determined in complex with porcine pancreatic trypsin in two crystalline forms. Twelve residues out of 181 in STI make contact with PPT in orthorhombic crystal structure while in tetragonal crystal structure, nine residues interact with PPT. However, the pattern for hydrogen bonding interactions involving the reactive loop residues is well conserved among two crystal forms, except that a hydrogen bond between Tyr-62 and Gly-96 is absent in tetragonal crystal structure. The P1 residue, Arg-63, makes most extensive hydrogen bonds with PPT, forming six hydrogen bonds in total and one ionic interaction with carboxylate group of Asp-189 in PPT [43]. Comparative analysis confirmed the more stable binding of ApKTI with TcPT and could be used as a potential drug against the stored grain pest. Further, it would be interesting to co-crystallize the two proteins and

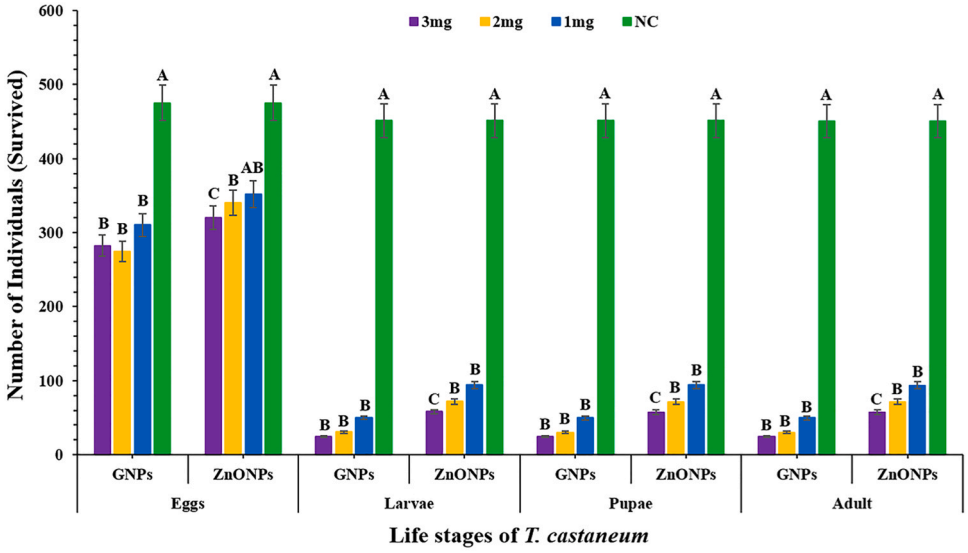

Fig. 8. : Comparison of two encapsulations for ApKTI. Composite graph is showing comparison of graphene and ZnO encapsulated ApKTI concentrations against *T. castaneum* along with negative control (NC; Tris-HCl, 100 mM, pH-7.6). Letters (A, B, C & D) above bars are indicating whether the treatment means are statistically significant or non-significant.

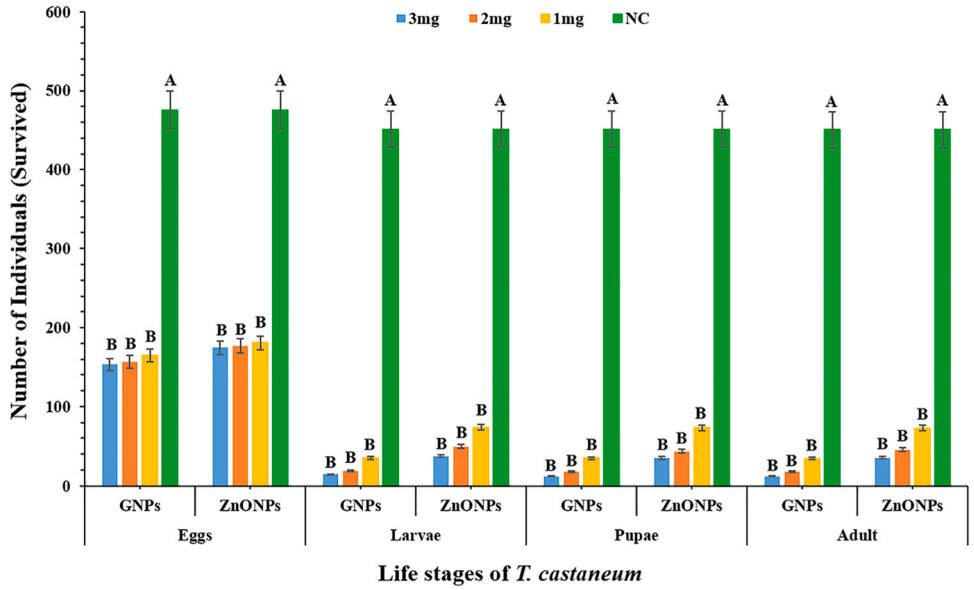

Fig. 9. : Comparison of two encapsulations for standard protein. Composite graph is showing comparison of graphene and ZnO encapsulated standard protein concentrations against *T. castaneum* along with negative control (NC; Tris-HCl, 100 mM, pH-7.6). Letters (A, B, C & D) above bars are indicating whether the treatment means are statistically significant or non-significant.

molecular structure of the complex should be observed to further decipher the potential and interactions between enzyme and inhibitor.

Molecular docking strongly favours the inhibitory interactions of ApKTI to TcPT, therefore; native ApKTI (3 mg/ml; 75 μg/g of wheat flour) was applied on *T. castaneum* diet in order to target its gut trypsin for mortality. ApKTI produced significant mortality in comparison to negative control. Previously, *Macuna pruriens* trypsin inhibitor exhibited inhibitory effect on the growth of melon fruit fly larvae (64–72 h old) and increased the larval mortality with increase in concentration from 0.2 μg to 625 μg/ml [44]. Similarly, larvae of *Helicoverpa armigera* fed on an artificial diet containing 150 μg/ml and 300 μg/ml *Solanum surattense* trypsin inhibitor exhibited negative impact on insect development in terms of mean larval weight, larval fertility, survival rate and nutritional indices [45]. Similar to this study, a Kunitz-type trypsin inhibitor from *Poincianella pyramidalis* seeds showed insecticidal potential in *Anagasta kuehniella* larval performance at two concentrations (0.25 % and 1 %: w/w) that caused mortality by direct inhibition of midgut enzymes [46]. Another *Piptadenia moniliformis* Kunitz-type trypsin inhibitor showed strong deleterious effects on the mass and survival of *Ceratitis capitata* during larval development. Larval mass was reduced by 50 % and mortality was also 50 % at a level of 0.3 % and 0.37 % (w/w) respectively [47].). Conclusively, ApKTI produced more mortality and potential in comparison to other reported KTI treatments. PIs are proteins or peptides that inhibit the catalytic action of proteases by forming stoichiometric complexes with their target enzymes, blocking or altering the active site. Such inhibition mechanism has been observed with digestive proteases of some insects leading to decreased or complete interruption of the dietary protein digestion, which is essential to make the amino acids available for larval growth and development. Thus, such potent molecules (ApKTI) can also be used as synthetic formulations for the growth reduction of stored grain insect pest like *T. castaneum*.

GNPs and ZnONPs encapsulated ApKTI enhanced significantly the insecticidal potential against *T. castaneum* in comparison to native protein. Additionally, GNPs (1–10 nm) encapsulated protein showed 67 % more significant mortality as compared to ZnONPs (30–150 nm) encapsulated ones. GNPs showed better mortality by the virtue of their smaller sizes which help them to extend the half-life of the drug and improve the penetration efficiency of the drug [48]. In general, smaller particles have a relatively large surface area as compared to larger ones; this increases the interaction with biological elements and consequently trigger more toxic and adverse effect [49]. Encasing the protein on ZnONPs and GNPs through physical interactions improves the stability, controlled release, and targeted distribution of Kunitz-type trypsin inhibitors (KTIs). The nanoparticles stay active in the treated seeds during the whole process to the insect's gut, preventing harmful effects from environmental variables and enzymes found in the gastrointestinal tract of insects. They improve the concentration and availability of KTI at the site of action by permitting efflux over the intestinal membrane. Additionally, enhanced cellular endocytosis indicates that there is more inhibitor within the cellular compartment to block trypsin, and the prolonged release from nanoparticles maintains enough KTI concentration steadily. These processes ensure a greater entomotoxic effect in comparison to the native protein, resulting in an increased impact. Despite great achievements in the emerging field of nano-biotechnology, an inclusive understanding of comprehensive cell interaction with NPs is yet to be accomplished. In-depth knowledge of such phenomenon may assist in design of more robust targeted therapeutic systems.

Apart from plant's natural defense mechanism of using these PIs against such herbivores insects, such potent molecules (ApKTI) can also be used as synthetic formulations for the growth reduction of phytophagous insects by inhibiting their digestive proteases of midgut such as trypsin, chymotrypsin, and other similar enzymes; thus, leading to poor digestion and availability of essential amino acids resulting in starvation leading to death of the pest.

Author contributions

S.M. performed the experiments and wrote the manuscript. S.S.T. and M.R. participated in X-ray crystallographic work. S.A and Q.S helped in entomology work. N.B. and M.N.H. participated in the synthesis and characterization of nanoparticles, A.S. and B.K. assisted in bioinformatics analysis. M.I. and W.B.A. revised the manuscript. A.A. conceived the study, supervised the work and revised the manuscript.

CRediT authorship contribution statement

Wadi Brak Alonazi: Writing – review & editing, Funding acquisition. **Muhammad Ibrahim:** Writing – review & editing. **Soren Skou Thirup:** Supervision. **Ahmed Akrem:** Writing – review & editing, Supervision, Conceptualization. **Sohaib Mehmood:** Writing – original

draft, Validation, Methodology, Investigation, Conceptualization. **Qamar Saeed:** Resources, Formal analysis. **Maria Rafiq:** Writing – review & editing, Formal analysis. **Binish Khaliq:** Writing – review & editing, Formal analysis. **Muhammad Najam-ul Haq:** Writing – review & editing, Formal analysis. **Ahsan Saeed:** Formal analysis. **Nabila Bashir:** Investigation, Formal analysis. **Sarah Ahmed:** Formal analysis.

Declaration of Competing Interest

The authors declare the following financial interests/personal relationships which may be considered as potential competing interests, Dr. Ahmed Akrem reports a relationship with Bahauddin Zakariya University that includes: employment. If there are other authors, they declare that they have no known competing financial interests or personal relationships that could have appeared to influence the work reported in this paper.

Acknowledgments

We are thankful to Higher Education Commission (HEC) of Pakistan for awarding IRSIP scholarship and Department of Molecular Biology and Genetics, Aarhus University, Aarhus, Denmark for granting access to the X-ray crystallography setup and King Saud University, Riyadh, Saudi Arabia for the support of this publication by Researchers Supporting Project (RSP2024R332).

Appendix A. Supporting information

Supplementary data associated with this article can be found in the online version at doi:10.1016/j.csbj.2024.07.023.

References

[1] Kuyu CG, et al. Evaluation of different grain storage technologies against storage insect pests over an extended storage time. J Stored Prod Res 2022;96:101945.
[2] Wicochea-Rodríguez JD, et al. A new green insecticide for stored wheat grains: efficiency against Rhyzopertha dominica and risk assessment. J Cereal Sci 2021;101:103312.
[3] Kumar S. Biopesticides: a need for food and environmental safety. J Biofertil Biopestic 2012;3(4):1–3.
[4] Mahmood I, et al. Effects of pesticides on environment. Plant, Soil Microbe: Vol 1: Implic Crop Sci 2016:253–69.
[5] Ngegba PM, et al. Use of botanical pesticides in agriculture as an alternative to synthetic pesticides. Agriculture 2022;12(5):600.
[6] Lengai GM, Muthomi JW, Mbega ER. Phytochemical activity and role of botanical pesticides in pest management for sustainable agricultural crop production. Sci Afr 2020;7:e00239.
[7] Srinivasan A, et al. A Kunitz trypsin inhibitor from chickpea (Cicer arietinum L.) that exerts anti-metabolic effect on podborer (Helicoverpa armigera) larvae. Plant Mol Biol 2005;57:359–74.
[8] Okedigba AO, et al. Comparative binding affinity analysis of soybean meal bowman-birk and kunitz trypsin inhibitors in interactions with animal serine proteases. ACS Food Sci Technol 2023;3(8):1344–52.
[9] Rodríguez-Sifuentes L, et al. Legumes protease inhibitors as biopesticides and their defense mechanisms against biotic factors. Int J Mol Sci 2020;21(9):3322.
[10] Rodrigues SM, et al. Nanotechnology for sustainable food production: promising opportunities and scientific challenges. Environ Sci: Nano 2017;4(4):767–81.
[11] Gilbertson LM, et al. Guiding the design space for nanotechnology to advance sustainable crop production. Nat Nanotechnol 2020;15(9):801–10.
[12] Zhu H, et al. Avermectin loaded carboxymethyl cellulose nanoparticles with stimuli-responsive and controlled release properties. Ind Crops Prod 2020;152:112497.
[13] Gao Y, et al. Metal-organic framework nanohybrid carrier for precise pesticide delivery and pest management. Chem Eng J 2021;422:130143.
[14] Wais U, et al. Nanoformulation and encapsulation approaches for poorly water-soluble drug nanoparticles. Nanoscale 2016;8(4):1746–69.
[15] Zhang Y, et al. Star polymer size, charge content, and hydrophobicity affect their leaf uptake and translocation in plants. Environ Sci Technol 2021;55(15):10758–68.
[16] Athanassiou C, et al. Nanoparticles for pest control: current status and future perspectives. J Pest Sci 2018;91:1–15.
[17] Jiang Q, et al. A nanocarrier pesticide delivery system with promising benefits in the case of dinotefuran: Strikingly enhanced bioactivity and reduced pesticide residue. Environ Sci: Nano 2022;9(3):988–99.
[18] Chung S, Revia RA, Zhang M. Graphene quantum dots and their applications in bioimaging, biosensing, and therapy. Adv Mater 2021;33(22):1904362.
[19] Pei X, et al. PEGylated nano-graphene oxide as a nanocarrier for delivering mixed anticancer drugs to improve anticancer activity. Sci Rep 2020;10(1):1–15.
[20] Meruvu H, et al. Synthesis and characterization of zinc oxide nanoparticles and its antimicrobial activity against Bacillus subtilis and Escherichia coli. Rasayan J Chem 2011;4(1):217–22.
[21] Fielden MR, et al. In silico approaches to mechanistic and predictive toxicology: an introduction to bioinformatics for toxicologists. Crit Rev Toxicol 2002;32(2):67–112.
[22] Malathi K, Ramaiah S. Bioinformatics approaches for new drug discovery: a review. Biotechnol Genet Eng Rev 2018;34(2):243–60.
[23] Laemmli UK. Cleavage of structural proteins during the assembly of the head of bacteriophage T4. Nature 1970;227(5259):680–5.
[24] Desjardins P, Conklin D. NanoDrop microvolume quantitation of nucleic acids. JoVE (J Vis Exp) 2010;45:e2565.
[25] Hewick RM, et al. A gas-liquid solid phase peptide and protein sequenator. J Biol Chem 1981;256(15):7990–7.
[26] Kabsch W. xds. Acta Crystallogr Sect D: Biol Crystallogr 2010;66(2):125–32.
[27] Liebschner D, et al. Macromolecular structure determination using X-rays, neutrons and electrons: recent developments in Phenix. Acta Crystallogr Sect D: Struct Biol 2019;75(10):861–77.
[28] Emsley P, et al. Features and development of Coot. Acta Crystallogr Sect D: Biol Crystallogr 2010;66(4):486–501.
[29] Desta IT, et al. Performance and its limits in rigid body protein-protein docking. Structure 2020;28(9):1071–81. e3.
[30] Erlanger BF, Kokowsky N, Cohen W. The preparation and properties of two new chromogenic substrates of trypsin. Arch Biochem Biophys 1961;95(2):271–8.
[31] Halstead D. Biological studies on species of Palorus and Coelopalorus with comparative notes on Tribolium and Latheticus (Coleoptera: Tenebrionidae). J Stored Prod Res 1967;2(4):273–313.
[32] Hummers Jr WS, Offeman RE. Preparation of graphitic oxide. J Am Chem Soc 1958;80(6). 1339-1339.
[33] Goyal B, Verma NK. Synthesis and Characterization of Pure Zinc Oxide Nanoparticles by Precipitation Method. Int J Eng Manag Res (IJEMR) 2015;5(2):386–9.
[34] McGraw-Hill, C., *Statistix 8.1 (Analytical Software, Tallahassee, Florida)*. Maurice/Thomas text, 2008.
[35] Dong Y, et al. Graphene quantum dots, graphene oxide, carbon quantum dots and graphite nanocrystals in coals. Nanoscale 2014;6(13):7410–5.
[36] Li Y, et al. ZnO/carbon quantum dots heterostructure with enhanced photocatalytic properties. Appl Surf Sci 2013;279:367–73.
[37] Zhou Z, et al. Distinctive roles of graphene oxide, ZnO quantum dots, and their nanohybrids in anti-corrosion and anti-fouling performance of waterborne epoxy coatings. Chem Eng J 2022;439:135765.
[38] Wahab R, et al. Photocatalytic oxidation of acetaldehyde with ZnO-quantum dots. Chem Eng J 2013;226:154–60.
[39] de Barros KMA, et al. A new Kunitz trypsin inhibitor from Erythrina poeppigiana exhibits antimicrobial and antibiofilm properties against bacteria. Biomed Pharmacother 2021;144:112198.
[40] Mehmood S, et al. Model prediction of a Kunitz-type trypsin inhibitor protein from seeds of Acacia nilotica L. with strong antimicrobial and insecticidal activity. Turk J Biol 2020;44(4):188–200.
[41] Zhou D, et al. Crystal structures of a plant trypsin inhibitor from Enterolobium contortisiliquum (EcTI) and of its complex with bovine trypsin. PLoS One 2013;8(4):e62252.
[42] Patil DN, et al. Structural basis for dual inhibitory role of tamarind K unitz inhibitor (TKI) against factor X a and trypsin. FEBS J 2012;279(24):4547–64.
[43] Song HK, Suh SW. Kunitz-type soybean trypsin inhibitor revisited: refined structure of its complex with porcine trypsin reveals an insight into the interaction between a homologous inhibitor from Erythrina caffra and tissue-type plasminogen activator. J Mol Biol 1998;275(2):347–63.
[44] Singh D, Kesavan AK, Sohal SK. Deterioration of digestive physiology of Bactrocera cucurbitae larvae by trypsin inhibitor purified from seeds of Mucuna pruriens. Pestic Biochem Physiol 2020;169:104647.
[45] Herwade AP, et al. In vivo developmental studies of Helicoverpa armigera and in silico molecular interactions with trypsin reveal the bio-insecticidal potential of trypsin inhibitor (SSTI) isolated from Solanum surattense. Int J Biol Macromol 2022;223:335–45.
[46] Guimarães LC, et al. Purification and characterization of a Kunitz inhibitor from Poincianella pyramidalis with insecticide activity against the Mediterranean flour moth. Pestic Biochem Physiol 2015;118:1–9.
[47] Cruz AC, et al. Bioinsecticidal activity of a novel Kunitz trypsin inhibitor from Catanduva (Piptadenia moniliformis) seeds. Plant Physiol Biochem 2013;70:61–8.
[48] Etter EL, Mei K-C, Nguyen J. Delivering more for less: nanosized, minimal-carrier and pharmacoactive drug delivery systems. Adv Drug Deliv Rev 2021;179:113994.
[49] Shang L, Nienhaus K, Nienhaus GU. Engineered nanoparticles interacting with cells: size matters. J Nanobiotechnology 2014;12(1):1–11.